Weathering of limestone after several decades in an urban environment

Mandana Saheb, Anne Chabas, Jean-Didier Mertz, Estel Colas, Olivier Rozenbaum, Jean-Pierre Sizun, Sophie Nowak, Lucile Gentaz, Aurélie Verney-Carron

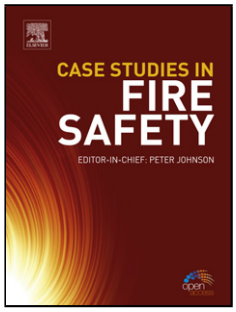

Title: Weathering of limestone after several decades in an urban environment

Author: Mandana Saheb Anne Chabas Jean-Didier Mertz Estel Colas Olivier Rozenbaum Jean-Pierre Sizun Sophie Nowak Lucile Gentaz Aurélie Verney-Carron

PII: S0010-938X(16)30287-6
DOI: http://dx.doi.org/doi:10.1016/j.corsci.2016.06.015
Reference: CS 6823

To appear in:

Received date: 8-2-2016
Revised date: 13-6-2016
Accepted date: 14-6-2016

Please cite this article as: Mandana Saheb, Anne Chabas, Jean-Didier Mertz, Estel Colas, Olivier Rozenbaum, Jean-Pierre Sizun, Sophie Nowak, Lucile Gentaz, Aurélie Verney-Carron, Weathering of limestone after several decades in an urban environment, Corrosion Science http://dx.doi.org/10.1016/j.corsci.2016.06.015

Weathering of limestone after several decades in an urban environment

Mandana Saheb [1*], Anne Chabas [1], Jean-Didier Mertz [2], Estel Colas [2], Olivier Rozenbaum [3], Jean-Pierre Sizun [4], Sophie Nowak [5], Lucile Gentaz [1], Aurélie Verney-Carron [1]

[1] LISA, UMR CNRS 7583, Université Paris-Est Créteil and Université Paris-Diderot, 61 avenue du Général de Gaulle, 94010 Créteil Cedex France
[2] CRC-LRMH, USR 3224, 29 rue de Paris, 77420 Champs-sur-Marne, France
[3] ISTO, UMR 7327, 1A rue de la Férollerie, 45100 Orléans, France
[4] Laboratoire Chrono-environnement UMR CNRS 6249, Univ. Bourgogne Franche-Comté, 25000 Besançon, France
[5] Plateforme Rayons X, UFR de Chimie, Université Paris-Diderot, 15 rue Jean-Antoine de Baïf, 75205 Paris Cedex 13, France

[*]**Corresponding author,** email : mandana.saheb@lisa.u-pec.fr

Highlights

The chemical and physical parameters of limestone exposed during more than 60 years in an urban environment are characterized at different scales.
From a chemical point of view, the alteration leads to an in-depth sulfur enrichment neoformation of gypsum and to a surface carbon deposit.
The weathering rate is highly dependent on the position of the block on the monument.

Abstract

The alteration of "Saint-Maximin Roche fine" limestones exposed to the Parisian urban environment during more than 60 years has been studied. It leads to changes of the texture and morphology, to the neo-formation of gypsum on the subsurface and to the deposition of carbon containing phases on the surface. Depending on the location of the blocks on the monuments, the alteration states are different related to different water activities that could influence the further alteration processes. The multiscale characterization has enabled to correlate the macrometric properties to the mesoscopic behavior, what is essential to understand the alteration mechanisms.

Keywords: A. stonework; B. SEM; B. Raman spectroscopy; B. XRD; C. atmospheric corrosion

Introduction

In many countries, the preservation of the building heritage is a cultural and scientific challenge. Therefore, the weathering processes of stone building materials have been widely studied on different materials types evolving in various environments [1–3]. Indeed, the alteration of the materials depends on both parameters intrinsic and extrinsic, so that its study requires interdisciplinary knowledge on material and environmental sciences [4–7].

As far as the extrinsic parameters to the materials are concerned, first, the climate plays a role on the natural ageing of the buildings. Secondly in a polluted area, atmospheric pollution directly affects the evolution of materials due to the chemical reactions induced by dry [8] and wet [9] deposition and their alteration kinetics (i.e. [10]). For over 200 years, the increase in energy production has caused high

atmospheric emissions in the form of gaseous pollutants (SO_2, CO_2, NO_x) and particulate matter (PM). Gases cause an acidic deposit that could increase the materials dissolution and/or the crusts formation [11–13]. The most common phases observed on limestone samples exposed to an urban area are sulphate containing phases [10,14–17]. Among them, gypsum ($CaSO_4$, $2H_2O$) formation is due to the interaction between the atmospheric SO_2 and the calcite from the stone. SO_2 is oxidized in SO_3 which is dissolved by condensation water and leads to H_2SO_4 formation [18]. This product reacts with the Ca^{2+} (from the dissolution of the calcite) and leads to the gypsum formation. In Paris and Paris suburb, according to the air quality survey network Airparif, since the 1950s, the concentration of SO_2 has decreased from 360 $\mu g.m^{-3}$ to a low value of around 1 $\mu g.m^{-3}$ in the last years [19]. However, the maximum values have reached up to 750 $\mu g.m^{-3}$ in the 1990's. Such extreme events could also play a role on the ageing of the monuments. In the Parisian basin since the 1990's the PM10 maxima (particles less than 10 µm in diameter) values could be over 400 $\mu g.m^{-3}$ [20]. For instance, in March 2014, Paris and its suburbs have been affected by an especially high rate of particulate peaks. In the Paris urban environment, soot represents almost 90% of suspended particles and of deposed particles in number [21]. Chemically inert, graphite is organized in carbonaceous nanospheres (about 10 nm in diameter) called Black Carbon or Elemental Carbon. Coated on this graphitic nucleus, adsorbed hydrocarbons, volatile organic compounds (VOCs), sulphates and in lesser extent nitrates can be fixed [22]. This mixture of organic and inorganic products can cause the increase in soot hydrophilic property [23] and promote water fixation or catalytic sulfation reactions (e.g. [24]). Furthermore the environment at city scale plays a role on the ageing of the materials, but also the local environment directly affects the alteration. The alteration on a single building can be very different from one location to another. It depends on the exposition (sides sheltered or not from rain, exposed to sun radiations), the height (subject to capillary rise or not, different water composition in the upper part and in the lower part of the building), the architecture (sculptures, frontage, windows...)... (e.g. [25]). All these parameters need to be taken into consideration and classified to propose a study of the alteration as exhaustive as possible.

Concerning the intrinsic properties of the material, its chemical and physical composition plays a role on the water transfer (aqueous or vapour) and on the exchanges with the environment. In the case of porous materials, the properties of the pore network will influence the water transfer [26]. Water is the main alteration factor as it can react directly with the material (e. g. dissolution process) or convey the aggressive agents (e. g. gypsum formation induced by the dissolution of gaseous SO_2). Consequently, to determine its transfer mode inside the material is of primary importance for the study of the alteration.

Moreover, the pore network can be modified by dissolution or crystallization processes [11] that will influence the subsequent alteration. The chemical composition of the material will also influence the chemical reactions and their associated kinetics. Therefore, the alteration is expected to be different on pristine and weathered materials with modified altered zones. The nature and the location of these altered zones could play a significant role in the subsequent alteration (changes in kinetics) and evolve as a function of time.

In France, 52% of the stone buildings are made out of limestone, so that the preservation of this type of stone is of primary importance [27]. Thus, the present work belongs to an ongoing study aiming to understand the alteration processes on limestone exposed to an urban polluted area, such as the Parisian basin. We have selected a specific limestone type from different monuments that have evolved in the same urban environment (Paris and Paris suburb). This limestone is widely used for the restoration of historical monuments in France, especially in the Parisian basin, the so-called “Saint-Maximin roche fine” limestone. This limestone from the Lutetian period (43 Million years) is relatively homogeneous from a chemical and physical point of view. Though the pristine stone has already been studied by several authors [28–31], to our knowledge, few have been done on real samples exposed during a long period to an urban atmosphere. In this context we have identified the alteration patterns formed on different “Saint-Maximin roche fine” limestone samples that have evolved in the Parisian urban environment following a multiscale methodology. These alteration patterns have been compared in order to identify the role of the local conditions and propose a reaction scenario of the alteration.

1. Material and methods

1.1 Materials

Limestone at two different alteration stages has been studied: pristine material from quarries (Q) of Saint-Maximin (Oise, France) dealing as reference and samples from various monuments in Paris and Paris suburbs. Two stones from the “Basilique of Saint-Denis” (SD limestone, 12th c.), and the pre-Haussmannian monument of the “Comédie Française” (C limestone, 17th c.) have been selected. These stones are part of restoration stone blocks of the 2nd part of the 20th century (ca 1950) and no surface treatment has been applied since the replacement. The SD limestone has been collected on a west oriented wall at a 19 m height, so that it was exposed to rainfall but not to capillary rises. The C limestone was located at the first floor of the building and was also only subject to rainfall events. Thus

the materials from the buildings have been exposed during a comparable period to a similar environment and at different heights.

The morphology and the mineralogy of the samples have been observed directly on the surface, and on cross sections from mesoscopic to nanometre scales. Moreover, thin section performed for the double staining of pore network enabled petrographic observations.

1.2 Surface analyses

The limestone surface state has been characterized using complementary analytical tools, from macro- to micrometric scale. Rugosimetric measurements have been performed to determine the surface roughness of the stone that could have been influenced by the alteration processes (dissolution and/or phases precipitation). Moreover, the mineralogical composition of the stone and of the altered zones have been determined using macro- and microbeam surface analyses such as X-Ray Diffraction (XRD), Scanning Electron Microscopy coupled with Energy Dispersive X-ray Spectroscopy (SEM-EDS) and Raman microspectrometry (micro-Raman).

1.2.1 Roughness measurement

The surface roughness of the samples has been measured using an interferometric microscope VEECO NT1100. The data have been acquired at x5 magnitude on 100 randomly selected zones, corresponding to a 1 cm^2 surface that was large enough to be representative of the whole sample. An 800 µm vertical scanning has been selected in VSI mode (Vertical Scanning Interferometry) with a 1% modulation threshold. According to the Standard ISO25178 [32], the roughness is now defined by the 3D surface texture parameters. The amplitude parameters such as Sa (arithmetic surface roughness), Sq (quadratic surface roughness) replace the traditional Ra (arithmetic roughness) and Rq (quadratic roughness) previously used for the 2D quantification. However, a mean value such as those given by Sa or Sq does not reveal a clear difference between altered stone samples. Thus another amplitude parameter must be used. Defined in the Standard ISO25178 as the maximum height from the highest point to the deepest valley, the Sz gives a best estimation of the magnitude of the surface roughness and is a good indicator of the surface complexity. For each studied samples, 100 values of Sz were measured. In order to obtain a statistical distribution of the Sz, these data were fitted to a combination of normal modes using the least square iterative routine. This treatment allows to identify the

amplitude, the median value and the standard deviation of the different modes representing the number distribution of the roughness (dN/dSz expressed in % number per range of 50 µm of roughness).

1.2.2 Elemental and mineralogical characterization

The morphology and the elemental composition of the samples have been investigated with a tabletop low-vacuum SEM.

To identify the mineralogical composition of the alteration phases, PXRD (Powder X-Ray Diffraction) has been performed on the bulk samples using an Empyrean diffractometer from Panalytical equipped with a multichannel PIXcel 3D detector and a filtered-copper X-ray source (1.5418 Å). Typically, each pattern was recorded in the 10°-60° 2θ range (0.013° for 150 s). It should be noted that the sample is mounted on a five-axis cradle with motorized movements to obtain a perfectly plane position. The phases have been identified using the Inorganic Crystal Structure Database (ICSD) with a selection of the best correlation. The Highscore software has been used to evaluate the concentration of each phase by integrated intensity and Reference Intensity Ratio (RIR) value and provide semi-quantitative data. For samples mainly composed of calcite with a high porosity, the depth of the analyses is lower than 120 µm.

At a micrometric scale, micro-Raman measurements have been performed using an Invia reflex spectrometer from the Renishaw Company equipped with a frequency-doubled Nd YAG emitting at 532 nm. A 50× optical microscope LEICA objective focused the laser beam and collected the scattered light, providing a laser spot size on the samples less than 2 µm. A 2400 l/mm grating induced a spectral resolution of about 1 cm^{-1}. The laser power on the sample was about 100 µW to minimise any phase transformation due to the heat generated. As there is no official database for Raman spectra, the spectra were compared to data from the literature.

1.3 Cross section analyses

Observations on cross sections are essential for allowing a full overview of the material, from the altered surface to the pristine core and evaluating the thickness of the zone chemically and physically modified by the alteration. Thus, the mineralogy of the stone and the pore network that directly influences the water transfer have been investigated.

1.3.1 Pore network characterization

All samples have been characterized at different scales (from micrometer to nanometer scale) using complementary analytical tools: petrophysical measurements to determine the macroscopic properties of the limestone exposed to liquid water, double staining method of pore network in thin section to qualitatively estimate the trapped porosity and the one accessible to water at atmospheric pressure, Mercury Intrusion Porosimetry (MIP) to quantify the pore volume and the Pore Throat Size Distribution (PTSD), and X-ray tomography to quantify the trapped and the connected porosity and reveal the heterogeneity in the pore network.

Parameters linked to the stones storage and fluid transfer properties have been determined using classical petrophysical measurements. To ensure the reproducibility of the results and because of the significant petrographic heterogeneity of the stone at small scale, the measurements have been performed on three samples with a representative volume (a volume higher 10 cm^3 determined by pre-tests) which allowed overcoming the possible natural anisotropy and the lateral variations. The capillarity absorption coefficient A [33], the drying evaporation kinetics (measured at at 40% Relative Humidity (RH)) and the total porosity Nt [34] have been determined.

Qualitative visualization of the porosity has been investigated using a staining method of pore network in thin section. The method is based on the wetting of the stone by two different stained resins. The first one, a red stained resin plays the role of the wetting fluid and fills the 'free' or porosity accessible to wetting fluid during capillary wetting [35,36]. The red zones identified by optical microscopy correspond to the porosity accessible to the water of the sample in natural wetting conditions because the red stained resin presents the same surface tension and dynamic viscosity than liquid water. The fraction of the porosity which was not accessible to water during saturation represents the trapped porosity; this pore volume is blue stained in thin sections. Thus this analysis has allowed to approach with a qualitative method the free and the trapped porosity, to localise the porosity in the minerals, to characterize the hydrodynamic role of these two types of pores in the transfer properties of the stone and to follow the evolution of the nature and distribution of the pores in the stones as a function of climatic and/or environmental modification.

Quantification of the porosity has been performed by MIP using a Micromeritics® Autopore IV system in standard conditions. Because mercury is a non-wetting liquid, progressive saturation of the pore network within the mercury has been obtained by applying a controlled pressure on the mercury in the range of 0.035 to 206 MPa. MIP technique has allowed determining the pore throat radii corresponding

to the PTRD of the limestone in the range from 0.005 to 180 µm. The porosimetric distribution of the pores is described as the pore throat radii (R) as a function of the injected volume (dV/dlogR), following Standard ASTM D4404-10 [37].

Microtomography analyses have been performed using an industrial Computed Tomography device Nanotom 180NF (GE Phoenix X-Ray, Wunstorf, Germany). X-ray microtomography is a non-destructive 3 dimensional imaging technique which enables to investigate the interior of samples. Visual inspection of these 3D volumes gives some insight about microstructure, cracks localization, shape of the internal objects... Despite this qualitative observation is an interesting step, quantitative results are more often required when considering porous complex materials such as stones. Indeed, 3D image analysis is a powerful technique to evaluate the morphological, structural and topological characteristics of materials. Preprocessing and image analysis tools used in this article were described in details elsewhere [28,38,39]. On our samples, the 6 mm diameter plugs used have enabled to obtain 3 µm voxel size images. Multiple scans have allowed imaging the plug on a large depth: from the top surface down to 16 mm below this surface.

1.3.2 Elemental and mineralogical characterization on cross section

Samples have been embedded in epoxy resin and cut with a diamond wire saw using oil as a lubricant. Sections were then grinded with increasing grade SiC papers and polished with a diamond paste (3 µm) under water. Sections of the stone have been observed in order to identify the morphology of the neocrystallisations using SEM with a tabletop LV-SEM TM3030 Hitachi, a low-vacuum scanning electron microscope equipped with EDS system Quantax 70 EDS Bruker. For the measurements, an accelerating voltage of 15 kV and an accumulation time of 1800 seconds in charge-up reduction mode have been used.

2 Results

2.1 Quarry (Q) limestone: general pattern of the pristine limestone

2.1.1 Surface observations

The Q limestone presents a unimodal rugosimetric distribution of around 760 µm (±46 µm) in Sz that corresponds to a homogeneous distribution of a mesoscopic rugosimetry on the pristine sample (see Fig. 1). Concerning the mineralogical composition of the stone, XRD analyses on the surface (Fig. 2) indicate that the stone is mainly composed of calcite and quartz respectively present with 97% and 3% (Table 2) with a homogeneous grain distributions.

2.1.2 Cross sections observations

The studied limestone comes from the fine stone bench of Saint Maximin quarry (Oise, France). It corresponds to a beige and fine biocalcarenite forming a grainstone structure according to Dunham's classification. Microscopic observations on thin sections (Fig. 3) enabled to identify that this stone is composed of foraminifer's tests (mainly milioles), crinoid articles, Mollusca and shell fragments, pellets, micritic intraclasts and quartz grains. The cohesion of the rock is carried out by a slight overlapping of grains by pressure-dissolution, by a cement composed of acicular calcite forming a thin and more or less isopach edge around the elements and, to finish, by a syntaxial sparitic calcitic cement around crinoids. This stone belongs to middle Lutetian geological period (around 43 Million years ago).

X-ray tomography provides an estimation of the total macroporosity (Fig. 4) as the image resolution (voxel size=3 µm) does not allow the micropores observation. This macroporous volume value of around 24% is homogeneously spread in a 1 cm high sprue.

Based on MIP measurements, the pore throat radii distribution of the quarry limestone is bimodal with a main mode centered on 20 µm (mode 1) and a second lower mode centered on 0.15 µm (mode 2) (Fig. 5 and Table 1). Most of the pore spaces are accessible to capillary water (Table 1), as it has been evidenced with the petrophysical measurements (free porosity of 38.1±0.4%) and with the dominant red colour of the free pore network (Fig. 3). This latter is mainly composed of most of the macropores and all the micropores. The trapped porosity, less represented, corresponds to spherical blue macropores located in the central part of the largest pore spaces of the network and the macropores sheltered inside the foraminifera tests (Fig. 3).

The capillary imbibition (or water absorption) curve of the Q limestone (Fig. 6) shows two parts which evolution is proportional to the square root of time according to the Washburn's law [40]. The first part of the curve corresponds to the filling of the free porosity. This porosity accessible by capillary water is mostly represented by micropores and partially by macropores as it can be seen on the thin sections photograph (Fig. 3). The capillary coefficient "A" of 3.7±0.1 $g.cm^{-2}.h^{-0.5}$ (Table 1) indicates the weight increase coefficient during this first phase. The second part of this curve shows a lower slope and corresponds to the progressive filling of the macroporosity formerly filled with air. During the second phase, the trapped air dissolves and diffuses into water, following Fick's law, with a slower kinetics than the first one. According to Bousquié [41] and Mertz [42], the shape of the water absorption curve is typical of the one of a pore network that shows both a homogeneous pore size distribution and a homogeneous PTRD, corresponding to a good connectivity between pores. The pore network is

homogeneously distributed which is in agreement with the surface observations (random distribution of the calcite and quartz grains) and the X-ray tomographic observations (random distribution of the pores).

The evaporation curve of the Q limestone is typical of a general evaporation process with three phases (Fig. 7). During the first drying phase, the mass loss is linear as a function of time. This phase corresponds to a water desaturation at a constant flux. The capillary supply is sufficient to ensure the hydric continuity of the water from the depth to the surface of the stone. This latter remains wet during this first phase; then, the residual water amount in the porous media, which corresponds to the "critical water saturation", will evaporate either by capillary transfer to the surface inside the network. The second phase, nonlinear versus time, corresponds to a desaturation at a decreasing flux and to the field of "pendulum" water. The third phase, linear, is related to a desaturation at a constant flow which occurs when the surface of the stone dries. During this last stage, the evaporation is only carried out inside the stone by diffusion of water vapor through its porous network [43,44]. The evaporation curve of the quarry limestone shows these three phases: evaporation by hydraulic continuity, intermediate phase, evaporation by water diffusion. The corresponding critical saturation time is reached after 191 hours (h).

2.2 Comédie Française (C) limestone

2.2.1 Surface observations

The C limestone presents a bimodal rugosimetric distribution of around 730 µm (±27 µm) and 55 µm (±44 µm) in Sz (see Fig. 1). Though the highest value of the Sz is close to the one of pristine Q sample, the amplitude is lower on the C sample. SEM observations of the surface of the C limestone display evidence of dissolution processes with a characteristic fibrous morphology of the calcite (Fig. 8). Moreover, XRD on the surface of the sample highlights the presence of authigenic gypsum. The semi-quantification of the phases estimates around 76% of calcite, 12% of quartz and 12% gypsum (Fig. 2 and Table 2). Thus the ratio of calcite is lower than in a pristine sample, probably due to a dissolution process.

Consequently the apparition of a bimodal rugosimetric distribution could have been caused by the competition between dissolution and precipitation at the surface, the two alteration processes generating antagonist effects, such as the erosion of the higher tops and the aggradation of the pores located in the pits.

2.2.2 Cross sections observations

The porosities estimated by water porosimetry and mercury intrusion porosimetry are respectively around 41.7±2.1% and 40.4% respectively (Table 1). The macropores throat radius measured by MIP is 10 µm (versus 20 µm in the pristine Q limestone) and the micropores throat radius is 3 µm (versus 0.15 µm in the pristine Q limestone). As presented on Fig. 4, the porosity of the C sample evaluated by tomography gradually decreases from 20% on the surface to 15% between 6 and 9 mm under the surface. On the surface the pore network is mainly composed of free micropores as identified by observations using double stained method (Fig. 3). After this range, the porosity slightly increases to a stable value of about 21% from 11 mm up to 16 mm. In general, as it can be seen on Fig. 3, the volume of the free macroporosity is lower than in the pristine sample and an important trapped porosity is observed. It can be caused by an obstruction of the pores entries during the new-phases precipitation process. Actually, SEM observations coupled with EDS analyses on a section of the stone show the presence of sulphur enriched zones (Fig. 9). These zones are mostly located at the surface of the stone, in agreement with the observations of the pore network and XRD analyses (Fig. 2). Moreover, some sulphur-enriched cracks can be seen up to several millimetres below the surface.

The capillary imbibition curve of the C limestone shows a unimodal porous network (Fig. 6). The slope of the first zone is lower than that of the pristine Q sample as mentioned by the A coefficient (Table 1). The transition between the capillary and the diffusion regime occurs after $1h^{0.5}$ (~$0.5h^{0.5}$ for the Q limestone) with a more important imbibition (1.9 $g.cm^{-2}.h^{-0.5}$ versus 3.7 $g.cm^{-2}.h^{-0.5}$ for the Q limestone). It can be concluded that the alteration modified the property of capillary transfer of the C limestone at two levels: firstly, the imbibition kinetics decreases and secondly, a higher quantity of water penetrates in the weathered limestone.

The evaporation kinetics is organized in three phases as it is the case for the pristine Q limestone (Fig. 7) with a higher critical saturation time for the C limestone (256h) where the evaporation mainly occurs at the surface because of a good hydric continuity and less by water diffusion. This can be explained by the presence of sulphur-enriched zones near the surface of the C limestone.

2.3 Saint-Denis (SD) limestone

2.3.1 Surface observations

The SD limestone presents a trimodal rugosimetric distribution of around 730 µm (±27 µm), 546 µm (±29 µm) and 405 µm (±29 µm) in Sz (see Fig. 1). As in the C limestone, higher Sz is close with a lower amplitude than on the pristine Q sample.

The presence of gypsum (9%) containing zones has been evidenced using XRD (Fig. 2 and Table 2). The quantity of gypsum at the surface is lower than on the C limestone. Calcite and quartz are respectively at 73% and 18% (Table 2). Moreover, as presented on the microphotograph of the surface of the sample (Fig. 10), the surface of the SD limestone is grayish. The identification of these localized zones has required the use of a micro-focused technique such as Raman spectroscopy. It allowed identifying scytonemin (Raman bands: 270, 493, 574, 58, 1000, 1020, 1097, 1173, 1323, 1384, 1457, 1555, 1598, 1717 cm^{-1}) [45,46]) and graphite (Raman bands: 1362, 1611 cm^{-1}) (Fig. 10) that constitute a biofilm covering the surface of the stone. The high luminescence of the Raman spectrum is linked to the presence of organic carbon. Scytonemin is an aromatic organic molecule detected in other studies on limestone alteration and it is linked to a biological activity exposed to UV radiation or a polluted environment [46]. The urban area of Paris suburb is a suitable environment for the activity of such bio-organisms. The biocolonization of the surface by fungi has been evidenced by SEM observations (Fig. 11). Graphite is one of the main components of soot emitted during the combustion of diesel fuel in car engines, kerosene in aircraft engine or natural gas in bus engine. In the case of the SD limestone, this could promote a regular supply of atmospheric water outside of rainfall events contributing to a higher biolocolonization of the substrate.

Thus, the trimodal rugosimetric mode can be explained by the following hypothesis. The secondary mode (546 µm) can be induced by alteration processes generating antagonist effects. The first process is the erosion of the higher tops that has been evidenced using SEM observations (Fig. 11). The second process is the aggradation of the pores located in the pits. Moreover the apparition of a third mode (405 µm) can be caused by the obstruction of the pores by different phases, such as soot and scytonemin aggregates.

2.3.2 Cross sections observations

The porosities measured by water porosimetry and MIP are around 30.7±1.0% and from 27.6% (surface) to 33.9% (below 2 mm from the surface) (Table 1). The macropores throat radius measured by MIP is 10 µm and the micropores throat radius is 3.5 µm. It is in the same range as the C limestone.

The double stained method and the X-ray tomography analyses on the SD limestone allow distinguishing different zones as a function of the distance to the surface (Fig. 3 and Fig. 4). From the surface to 2 mm under the surface, the average porosity evaluated by tomography is 21%. The free porosity is mainly composed of micropores and macropores and the rare trapped porosity is principally composed of

macropores. Then, from 2 mm to 3.5 mm under the surface, the porosity drops to 4%. This zone is enriched in gypsum and mainly contains a trapped macroporosity becoming more and more important with depth. The free (red) porosity is reduced and mainly composed of the micropores. The presence of the gypsum containing zones has also been evidenced using SEM-EDS (Fig. 12) analyses on a cross section. From 11 mm below the surface, the stone presents a pattern similar to the pristine Q limestone, with an average porosity of 21%.

This specific local porosity directly influences the fluid transfer properties, as it has been identified with the petrophysical measurements (Table 1 and Fig. 6). From an imbibition kinetics point of view, the SD Limestone is more complex than the pristine Q and the C limestone. The usual two linear parts are subdivided in three steps. The first step corresponds to a very low A coefficient of 0.5±0.1 $g.cm^{-2}.h^{-0.5}$ (Table 1). The second step corresponds to an increase of the kinetics with a slope similar to that of the C limestone (A=2.4±0.4 $g.cm^{-2}.h^{-0.5}$). This can be interpreted by the imbibition of the microporosity enabled after the crossing of a kind of capillary barrier (porosity decrease in this zone). The third step, with the slowest slop, illustrates the filling of the residual macroporosity. In the SD limestone, the amount of water that can penetrate by capillarity is lower than on the other limestone samples. This indicates a highly modified porous network by the weathering. Two phenomena can occur at the same time: the filling of the porosity by new-formed products and the transformation of the free porosity into trapped porosity. The evaporation kinetics measurement (Fig. 7) reveals a shortened critical saturation time (122h). The surface of the SD limestone is dry after 5 days and the evaporation essentially occurs deep in the sample, by water diffusion. This is in good accordance with the presence of a pore blocking zone which also limits the evaporation towards the surface.

3 Discussion

Following former observations, the general pores structure on the pristine and weathered limestones has been evidenced and a schematic mechanism can be presented on Fig. 13 for both samples SD and C limestone.

On the pristine Q limestone, the morphology and distribution of the phases are homogeneous. The roughness is unimodal, pores are randomly distributed in the limestone and the main phases are calcite and quartz also randomly distributed in the stone. On the Comédie C limestone, dissolution processes of the calcite and precipitation of gypsum lead to a complexification of the texture and the chemical distribution of the phases. The modified zone from the alteration is of few millimetres (around 4 mm) under the surface. On the Saint-Denis SD limestone, dissolution and precipitation of gypsum, calcite and

soot deposit also induce a complexification of the texture and the chemical phases distribution in the limestone. The thickness of the modified layer is of around 8 mm.

Concerning the surface of the stone, the weathering has caused a decrease and a complexification of the roughness. From one mode, the roughness evolves to two and three modes (Fig. 1). In both cases, the amplitude between the highest peaks and the lowest pits decrease can be explained by an erosion by dissolution of the summits corresponding to the top of the calcite grains showing a fibrous morphology. The filling of the valleys is due to gypsum precipitation (essentially for the C limestone) and deposition of airborne particulate (soot) and biocolonization of fungi on the SD limestone. This biofilm is particularly favored by an important supply of water. Thus, the local environment plays an important role as the SD limestone is located at 19 m high in a zone exposed to rainfall.

In both cases, a sulfation process has been evidenced by a sulfur enrichment which decreases from the surface to the depth on the C limestone and that appears only between 2 and 3.5 millimeters deep on the SD limestone. This in-depth location is due to the influence of the water run-off which dissolves the SO_2 reactive zones formed between two rainy events. Indeed, this dissolution is particularly active in the top of the monuments which is exposed to a more acidic rain. The lower parts of the building are leached by a buffered rain, less aggressive that can explain the lower alteration on the Comédie limestone. For both weathered limestone samples, this sulfur enrichment acts as a barrier that slows down the capillary transfers. Depending on to the position of the barrier, the evaporation modes are different: on the C limestone, the evaporation mainly occurs on the surface and on the SD limestone, the in-depth reaction with SO_2 favors the evaporation by diffusion under the surface.

From a microscopic point of view, the reaction with SO_2 modifies the stone porous network. Indeed, when a pristine limestone is mainly composed of free porosity accessible by capillary transfer, the porous network shows an important trapped porosity after alteration. A possible explanation is the progressive transformation of the free macropores in trapped micropores due to gypsum precipitation at the surface of the grains (bioclast, intraclast…) or in the micritic or sparitic matrix that closes the exit point of the micropores and thus the access of liquid water.

4 Conclusions

This study identifies the alteration patterns formed on limestone from historical buildings exposed to an urban environment. Samplings have been carried out on two different monuments (Saint Denis Basilica and the Comédie) at different heights (top and medium level) respectively. After more than 60 years of exposure in Paris in unsheltered conditions, the “Saint-Maximin roche fine” limestone

used for restauration shows some modifications affecting the surface and the subsurface up to several millimeters in depth. The multiscale methodology has allowed to establish the links between nano- to micrometric observations and the macroscopic behavior of the stone. In every case, the alteration leads to a heterogenization of the limestone, in term of morphology (roughness and porosity) and phases distribution (precipitation of gypsum and deposition of carbon containing phases). Moreover depending on the location of the limestone block on the monuments, the alteration states are related to different water activities, with a higher alteration on the sample located higher on the monument. This highlights the importance of the local environment on the alteration kinetics.

5 Acknowledgement

The authors would like to thank the French Ministry for Culture and Communication for the financial support. Special thanks to Mr Chauvelier from Lanfry Company and Mr Debray from Dubocq Company for their decisive help during the sampling on the monuments. For the characterization measurements, the authors thank the SIS2M/LAPA for the Raman analyses.

References

[1] A.J. Hutchinson, J.B. Johnson, G.E. Thompson, G.C. Wood, P.W. Sage, M.J. Cooke, Stone degradation due to wet deposition of pollutants, Corros. Sci. 34 (1993) 1881–1898.

[2] S.J. Haneef, J.B. Johnson, G.E. Thompson, G.C. Wood, The degradation of coupled stones by wet deposition processes, Corros. Sci. 34 (1993) 497–510.

[3] T.T.N. Lan, R. Nishimura, Y. Tsujino, Y. Satoh, N. Thi Phuong Thoa, M. Yokoi, Y. Maeda, The effects of air pollution and climatic factors on atmospheric corrosion of marble under field exposure, Corros. Sci. 47 (2005) 1023–1038.

[4] P. Brimblecombe, C.M. Grossi, I. Harris, Future trends in surface wetness and relative humidity and potential impact on materials, Pollut. Atmos. (2007) 95–100.

[5] P. Brimblecombe, C.M. Grossi, I. Harris, Climate Change Critical to Cultural Heritage, Environ. Earth Sci. (2011) 195–205.

[6] C. Sabbioni, P. Brimblecombe, M. Cassar, The Atlas of Climate Change Impact on European Cultural Heritage: Scientific Analysis and Management Strategies, Anthem Press, 2010.

[7] W. Tang, C.I. Davidson, S. Finger, K. Vance, Erosion of limestone building surfaces caused by wind-driven rain: 1. Field measurements, Atmos. Environ. 38 (2004) 5589–5599.

[8] J.B. Johnson, M. Montgomery, G.E. Thompson, G.C. Wood, P.W. Sage, M.J. Cooke, The influence of combustion-derived pollutants on limestone deterioration: 1. The dry deposition of pollutant gases, Corros. Sci. 38 (1996) 105–131.

[9] J.B. Johnson, M. Montgomery, G.E. Thompson, G.C. Wood, P.W. Sage, M.J. Cooke, The influence of combustion-derived pollutants on limestone deterioration: 2. The wet deposition of pollutant species, Corros. Sci. 38 (1996) 267–278.

[10] D. Camuffo, M. Del Monte, C. Sabbioni, Origin and growth mechanisms of the sulfated crusts on urban limestone, Water. Air. Soil Pollut. (1993) 351–359.

[11] M. Reddy, S.I. Sherwood, B.R. Doe, Limestone and marble dissolution by acid rain: an onsite weathering experiment, Am. Chem. Soc. Symp. (1986) 226–238.

[12] C. Sabbioni, Mechanisms of air pollution damage to stone, The Effects of Air Pollution on the Built Environment, Air Pollut. Rev. (2003) 63–106.

[13] P. Ausset, Apports des expériences en chambre de simulation à la connaissance des effets de la pollution atmosphérique sur les pierres du patrimoine bâti, Pollut. Atmos. 49 (2007) 29–46.

[14] G. Zappia, C. Sabbioni, M.G. Pauri, G. Gobbi, Mortar damage due to airborne sulfur compounds in a simulation chamber, Mater. Struct. (1994) 469–473.

[15] H. Böke, S. Akkurt, Ettringite formation in historic bath brick–lime plasters, Cem. Concr. Res. 33 (2003) 1457–1464.

[16] M. Collepardi, Thaumasite formation and deterioration in historic buildings, Portland Limest. Cem. 21 (1999) 147–154.

[17] S.S. Potgieter-Vermaak, R.H.M. Godoi, R.V. Grieken, J.H. Potgieter, M. Oujja, M. Castillejo, Micro-structural characterization of black crust and laser cleaning of building stones by micro-Raman and SEM techniques, Spectrochim. Acta. A. Mol. Biomol. Spectrosc. 61 (2005) 2460–2467.

[18] P. Ausset, J.L. Crovisier, M. Del Monte, V. Furlan, F. Girardet, C. Hammecker, D. Jeannette, R.A. Lefevre, Experimental study of limestone and sandstone sulphation in polluted realistic conditions: The Lausanne Atmospheric Simulation Chamber (LASC), Atmos. Environ. 30 (1996) 3197–3207.

[19] Surveillance & information sur la qualité de l'air en Île-de-France - Bilan année 2015, Airparif, 2016.

[20] http://www.airparif.asso.fr/.

[21] A. Chabas, T. Lombardo, H. Cachier, M.H. Pertuisot, K. Oikonomou, R. Falcone, M. Verità, F. Geotti-Bianchini, Behaviour of self-cleaning glass in urban atmosphere, Build. Environ. 43 (2008) 2124–2131.

[22] H. Cachier, Carbonaceous combustion aerosols, in: Atmospheric Part., Wiley J. & Sons, Roy M. Harrison and René Van Grieken, London (1998) 295–348.

[23] O.B. Popovitcheva, M.E. Trukhin, N.M. Persiantseva, N.K. Shonija, Water adsorption on aircraft-combustor soot under young plume conditions, Atmos. Environ. 35 (2001) 1673–1676.

[24] P. Brimblecombe, C.M. Grossi, Aesthetic thresholds and blackening of stone buildings, Sci. Total Environ. 349 (2005) 175–189.

[25] M. Angeli, Multiscale study of stone decay by salt crystallization in porous networks - Etude multiéchelle de la dégradation des roches par la cristallisation de sels dans les réseaux poreux, Université de Cergy-Pontoise, 2007.

[26] D. Jeannette, Structure de porosité, mécanismes de transfert des solutions et principales altérations des roches de monuments, in: Pietra Dei Monum. Ambiente Fis. E Cult. (1994) 49–63.

[27] http://monumat.brgm.fr/.

[28] O. Rozenbaum, L. Barbanson, F. Muller, A. Bruand, Significance of a combined approach for replacement stones in the heritage buildings' conservation frame, Comptes Rendus Geosci. 340 (2008).

[29] G. Fronteau, C. Moreau, C. Thomachot-Schneider, V. Barbin, Variability of some Lutetian building stones from the Paris Basin, from characterisation to conservation, Eng. Geol. 115 (2010) 158–166.

[30] M. Angeli, J.-P. Bigas, B. Menendez, R. Hébert, C. David, Influence of capillary properties and evaporation on salt weathering of sedimentary rocks, in: Herit. Weather. Conserv., Taylor&Francis, Alvarez de Buego, Gomez Hera & Vasquez Cavo, Madrid, Spain (2006) 253–259.

[31] M. Angeli, D. Benavente, J.-P. Bigas, B. Menéndez, R. Hébert, C. David, Modification of the porous network by salt crystallization in experimentally weathered sedimentary stones, Mater. Struct. 41 (2007) 1091–1108.

[32] ISO 25178-2:2012, Geometrical product specifications (GPS) - Surface texture: Areal - Part 2: Terms, definitions and surface texture parameters, 2012.

[33] AFNOR Standard NF EN 1925, Natural stone test method - Determination of water absorption coefficient by capillarity, 1999.

[34] AFNOR Standard NF EN 1936, Natural stone tests, Determination of real density and apparent density and of total and open porosity, 1999.

[35] B. Zinszner, C. Meynot, Visualisation des propriétés capillaires des roches réservoirs, Rev. Inst. Fr. Pétrole. (1982) 337–361.

[36] B. Zinszner, F.-M. Pellerin, A Geoscientist's Guide to Petrophysics, Editions TECHNIP, 2007.

[37] ASTM D4404-10, Standard Test Method for Determination of Pore Volume and Pore Volume Distribution of Soil and Rock by Mercury Intrusion Porosimetry, 2010.

[38] O. Rozenbaum, 3-D characterization of weathered building limestones by high resolution synchrotron X-ray microtomography, Sci. Total Environ. 409 (2011) 1959–1966.

[39] O. Rozenbaum, S. Anne, J.-L. Rouet, Modification and modeling of water ingress in limestone after application of a biocalcification treatment, Constr. Build. Mater. 70 (2014) 97–103.

[40] E. Washburn, The Dynamics of Capillary Flow, Phys. Rev. (1921) 273–283.

[41] P. Bousquié, Texture et porosité de roches calcaires, Université Paris 6, 1979.

[42] J.D. Mertz, Structures de porosité et propriétés de transport dans les grès, Université Louis Pasteur de Strasbourg, 1991.

[43] J.F. Pearse, T.R. Oliver, D.M. Newitt, The mechanisms of drying of solids: I. The forces giving rise to movement of water in granular beds during drying, Trans. Inst. Chem. Eng. (1949) 1–8.

[44] C. Jouany, Transferts d'eau par evaporation dans les milieux argileux, Université Paul Sabatier (Toulouse 3), 1981.

[45] H.G. Edwards, F. Garcia-Pichel, E. Newton, D. Wynn-Williams, Vibrational Raman spectroscopic study of scytonemin, the UV-protective cyanobacterial pigment, Spectrochim. Acta. A. Mol. Biomol. Spectrosc. 56 (2000) 193–200.

[46] N. Prieto-Taboada, I. Ibarrondo, O. Gómez-Laserna, I. Martinez-Arkarazo, M.A. Olazabal, J.M. Madariaga, Buildings as repositories of hazardous pollutants of anthropogenic origin, J. Hazard. Mater. 248–249 (2013) 451–460.

Table of figures

Figure 1: Rugosimetric distribution of the Sz parameters on the pristine (Quarry Q) and weathered (Comédie C and Saint Denis SD) limestone. Sz is the maximum height from the highest point to the deepest valley and dN/dSz is the % number per range of 50 µm of roughness.

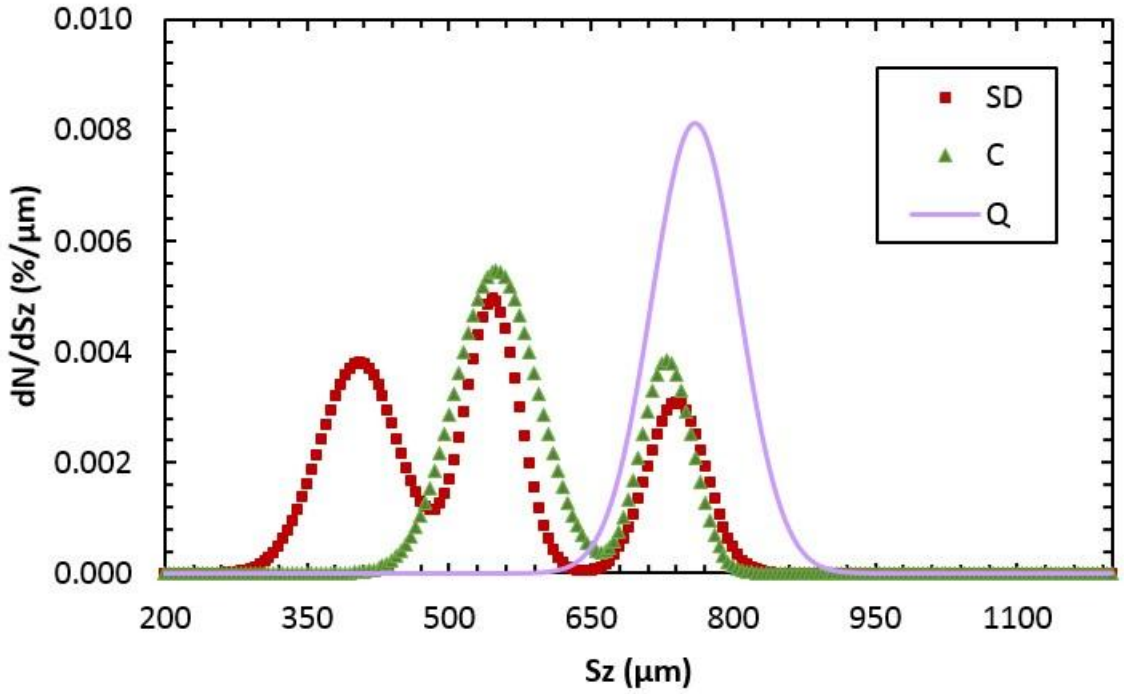

Figure 2: XRD analyses on the surface on the pristine (Quarry Q) and weathered (Comédie C and Saint Denis SD) limestone. Ca is for calcite (01-072-1937), Qz is for quartz (04-075-0443) and G is for gypsum (00-033-0311).

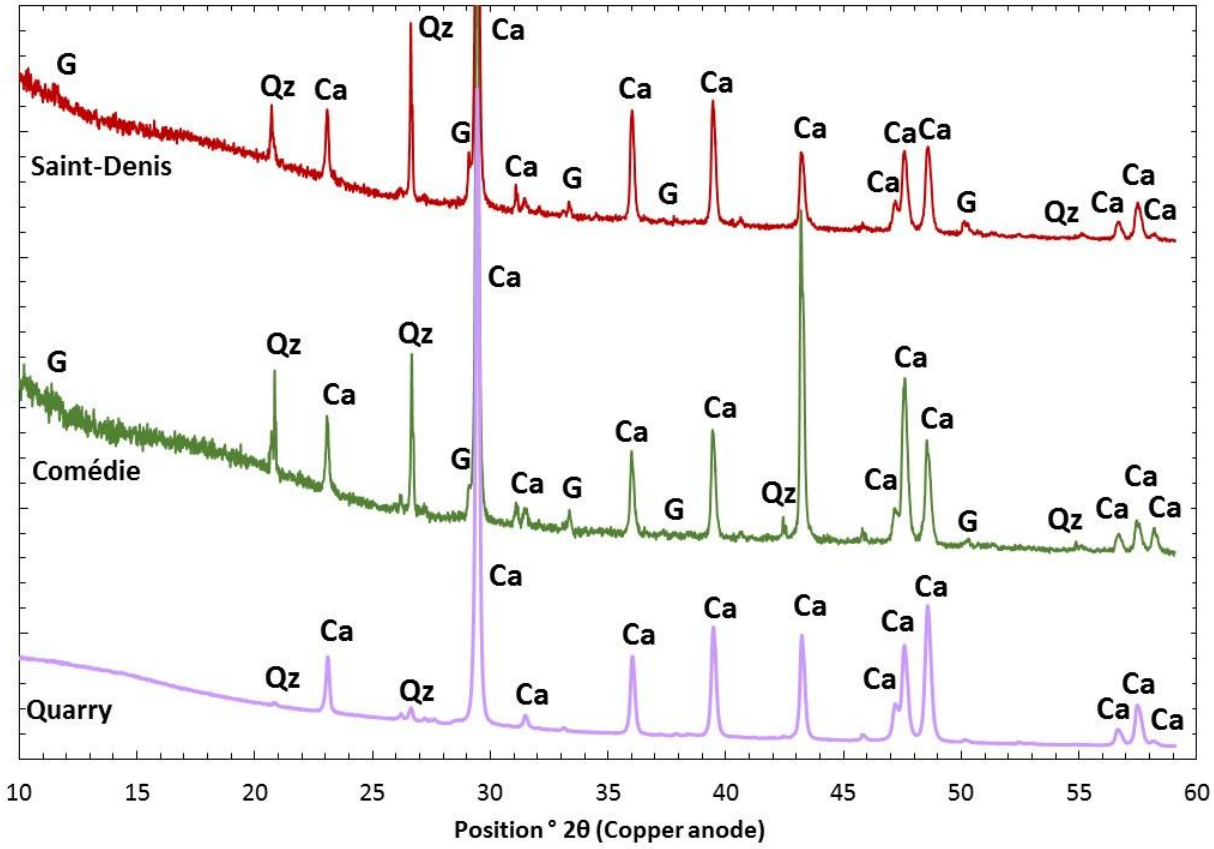

Figure 3: General view of free (red) and trapped (blue) pore distribution in the pristine limestone (Quarry Q) and the weathered (Comédie C and Saint Denis SD) limestones.

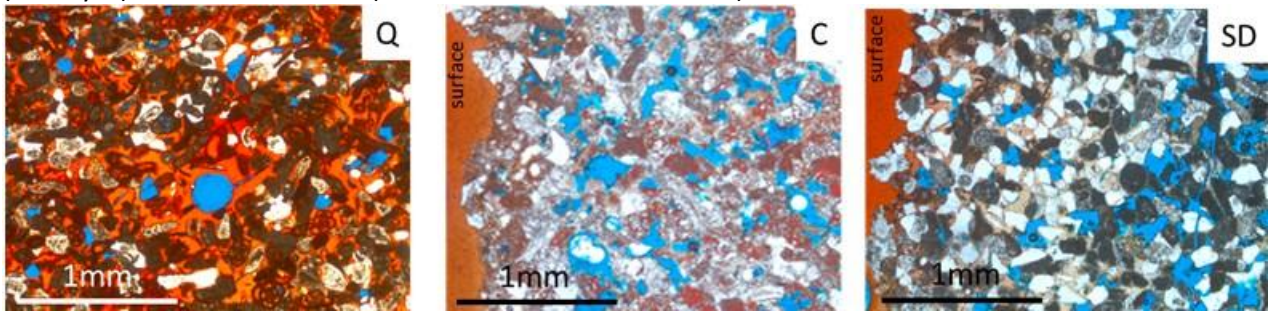

Figure 4: Porosity distribution in the pristine (Quarry Q) and weathered (Comédie C and Saint Denis SD) limestone as a function of the distance from the exposed surface.

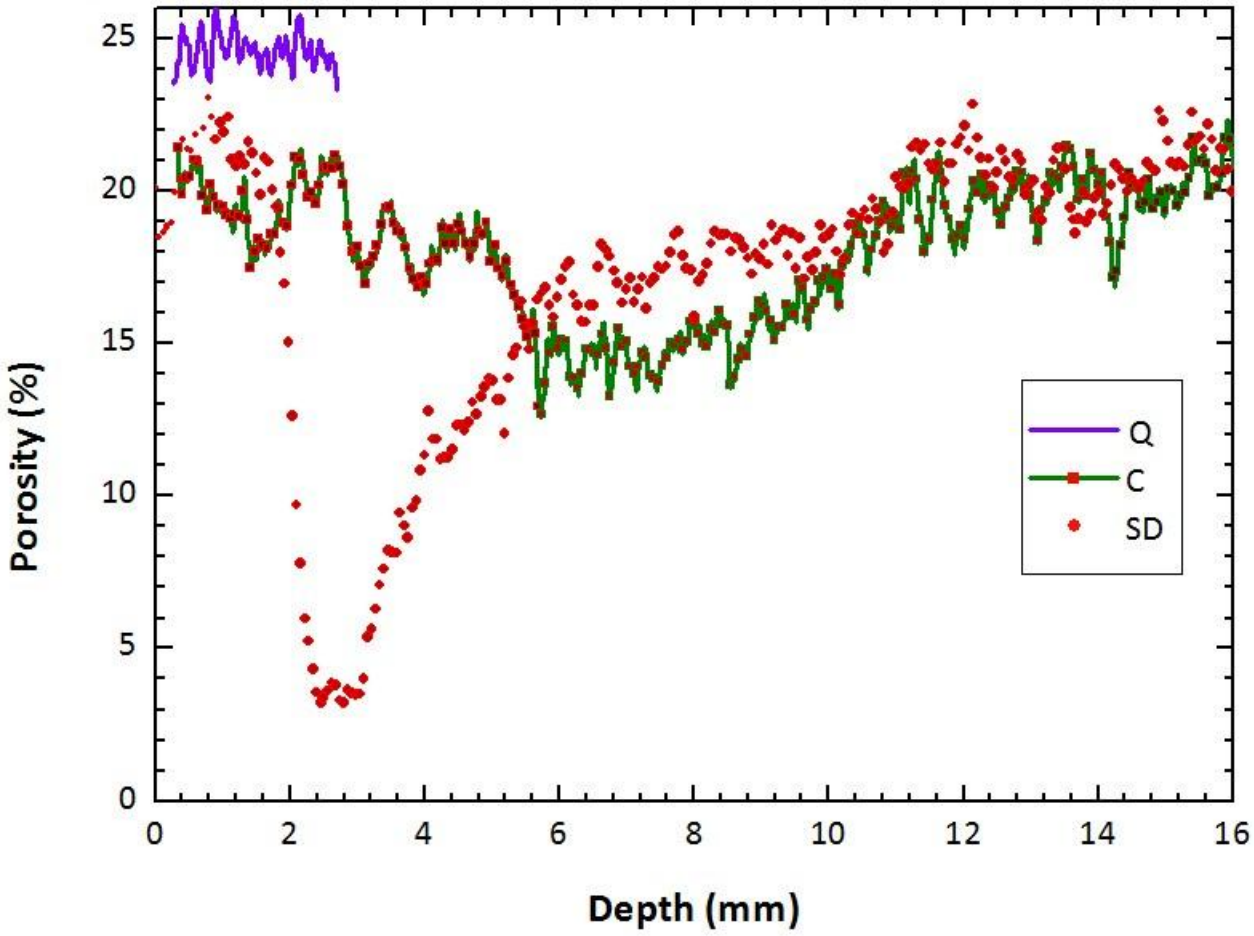

Figure 5: Pore throat radii distribution of pristine (Quarry Q) and weathered (Comédie C and Saint Denis SD) limestones. V is the injected volume of mercury and R is the pore throat radii.

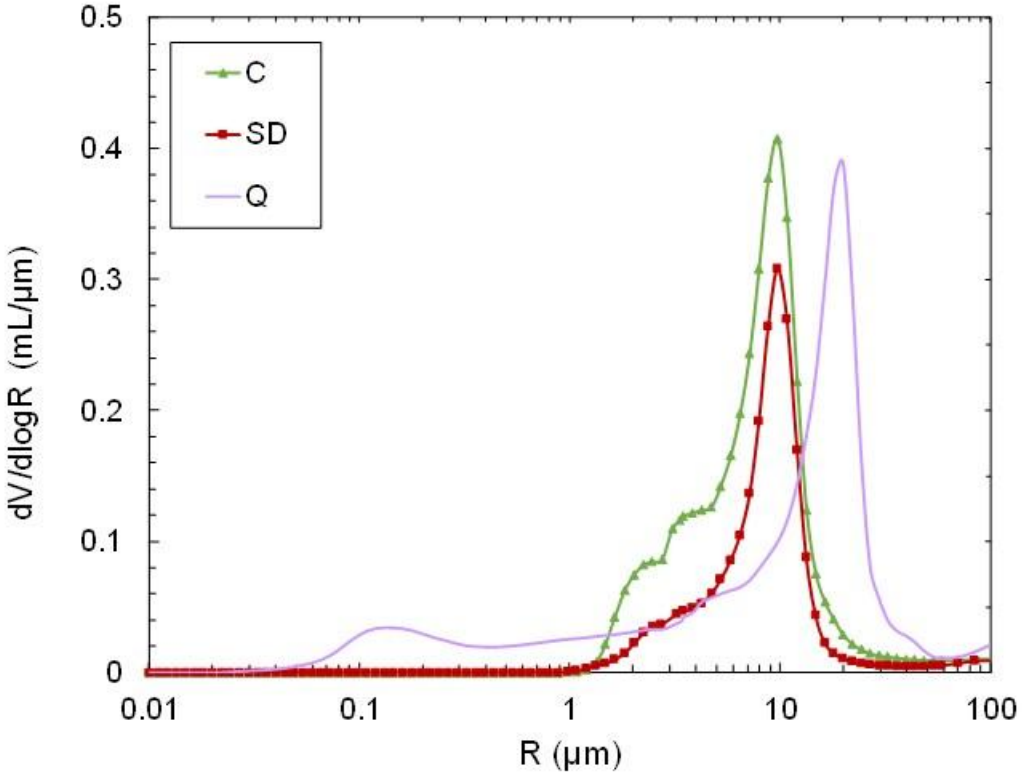

Figure 6: Capillary imbibition curves of pristine (Quarry Q) and weathered (Comédie C and Saint Denis SD) limestones. W is the weight of the sample, S is the surface exposed to water and t is the time.

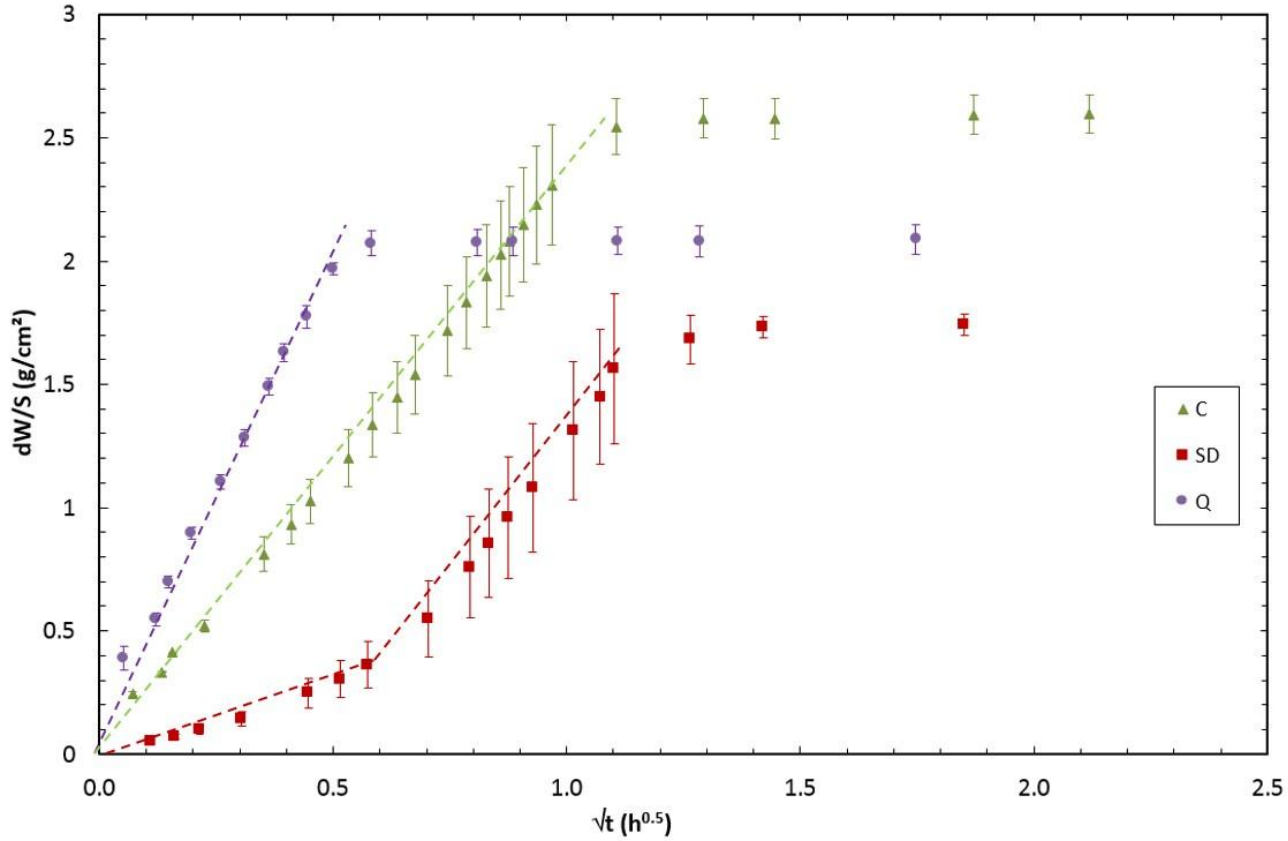

Figure 7: Evaporation kinetics curves of pristine (Quarry Q) and weathered (Comédie C and Saint Denis SD) limestones. Dashed lines correspond to critical saturation times. W is the weight of the sample, S is the surface exposed to water and t is the time.

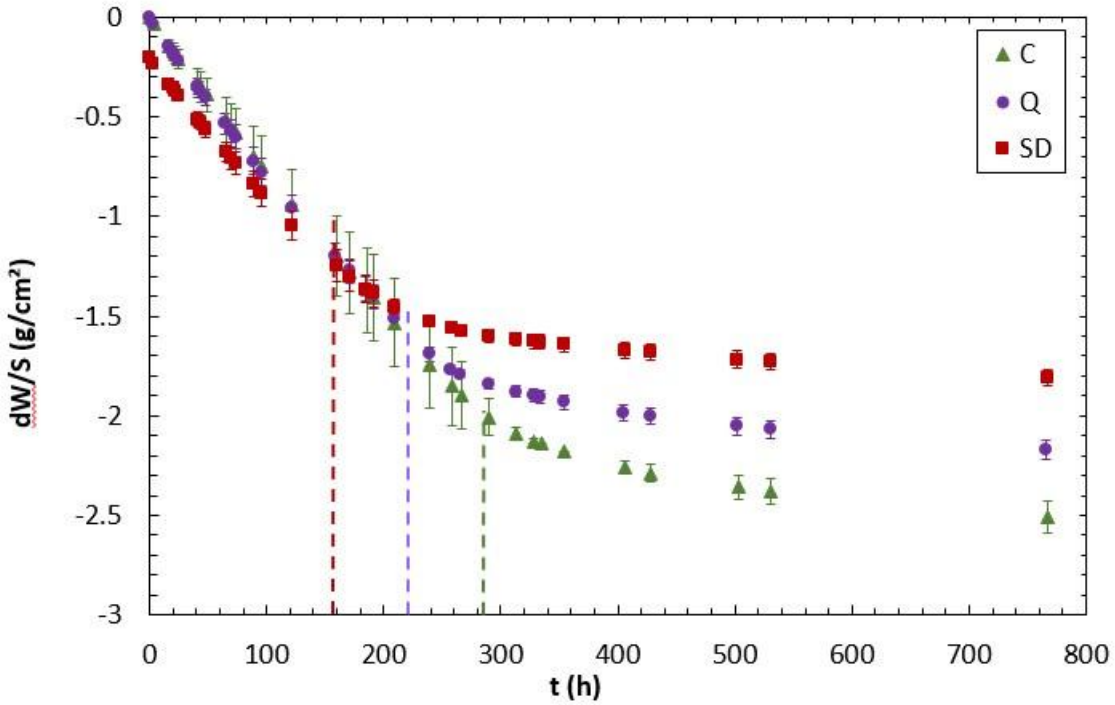

Figure 8: SEM observation of the surface of the Comédie C limestone

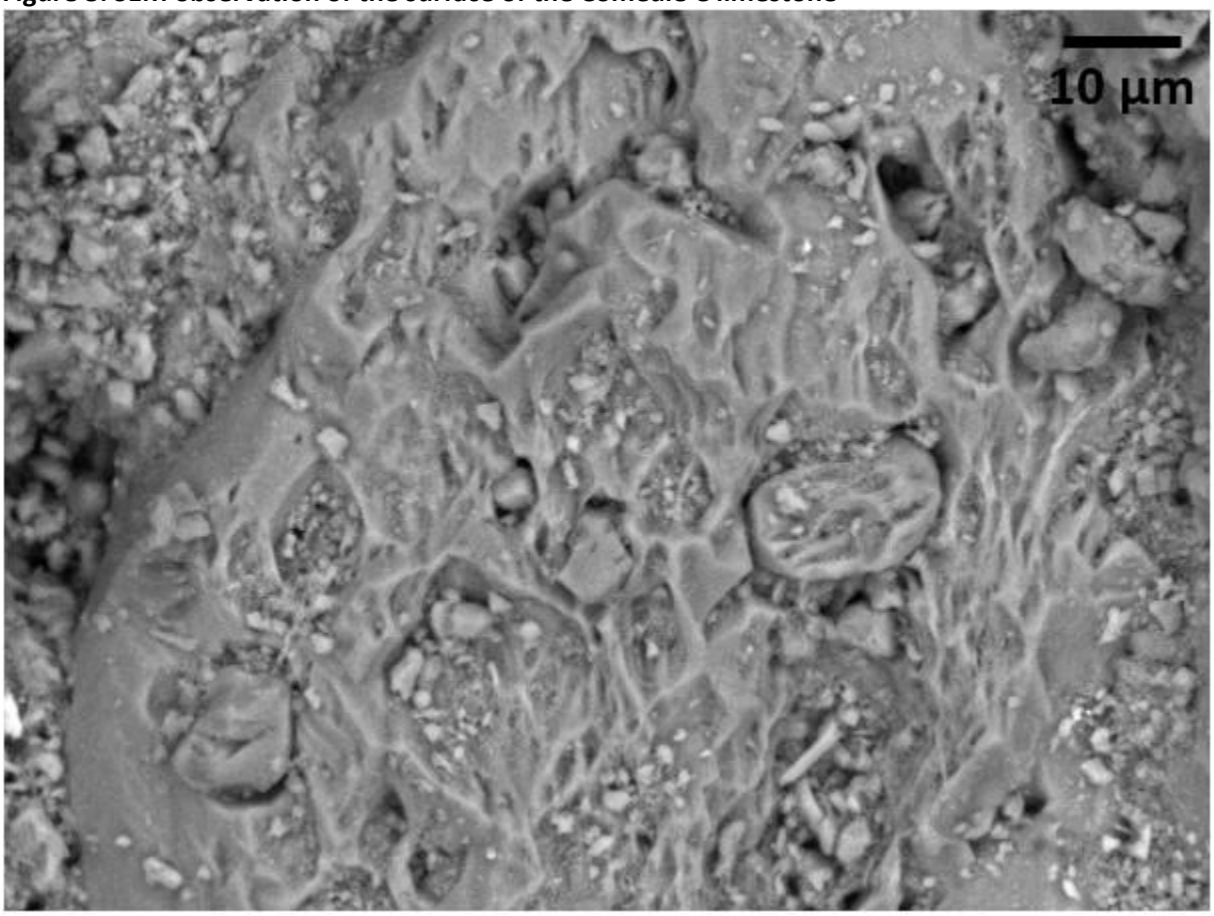

Figure 9: SEM image (BSE) of a cross section of the Comédie C sample and associated Kα mapping of S.

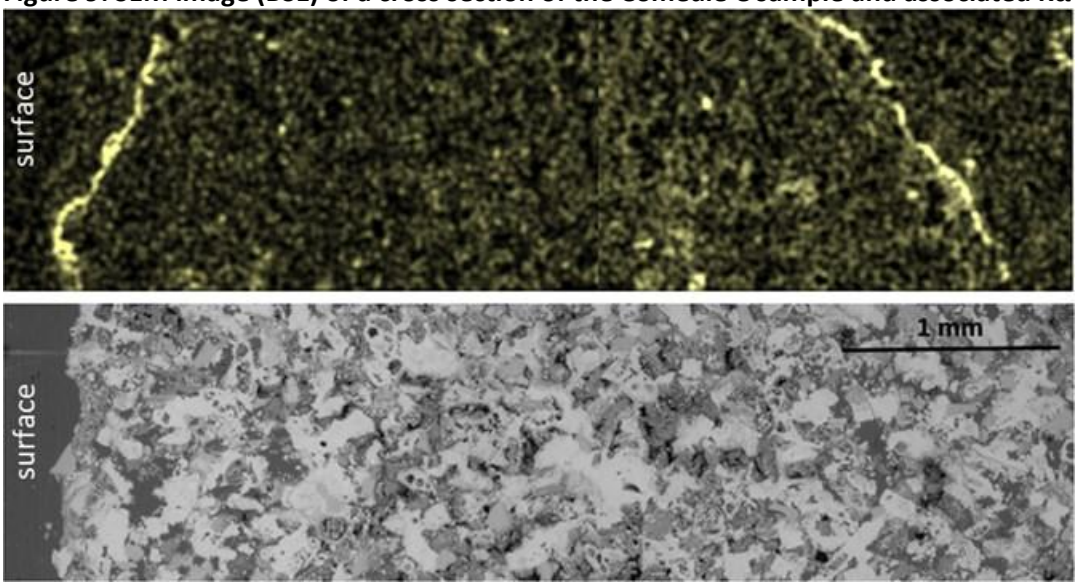

Figure 10: Optical micrograph on the limestone from Saint-Denis and associated Raman spectra (λ=532 nm).

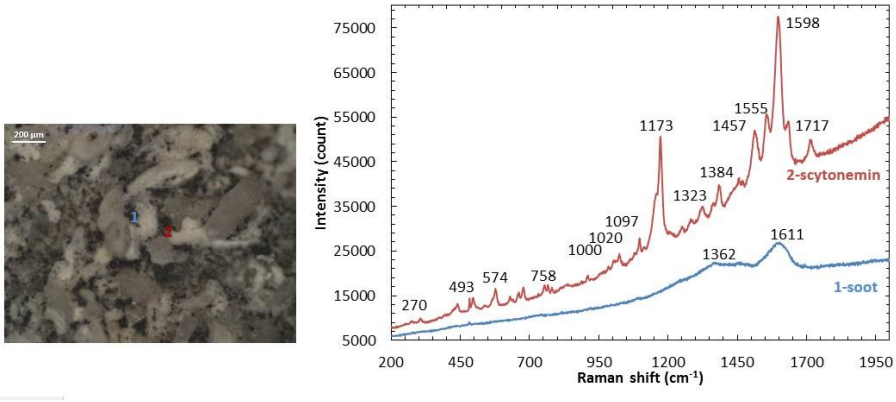

Figure 11: SEM observation of the surface of the Saint-Denis SD limestone. A: zone of calcite dissolution, B: biocolonized zone.

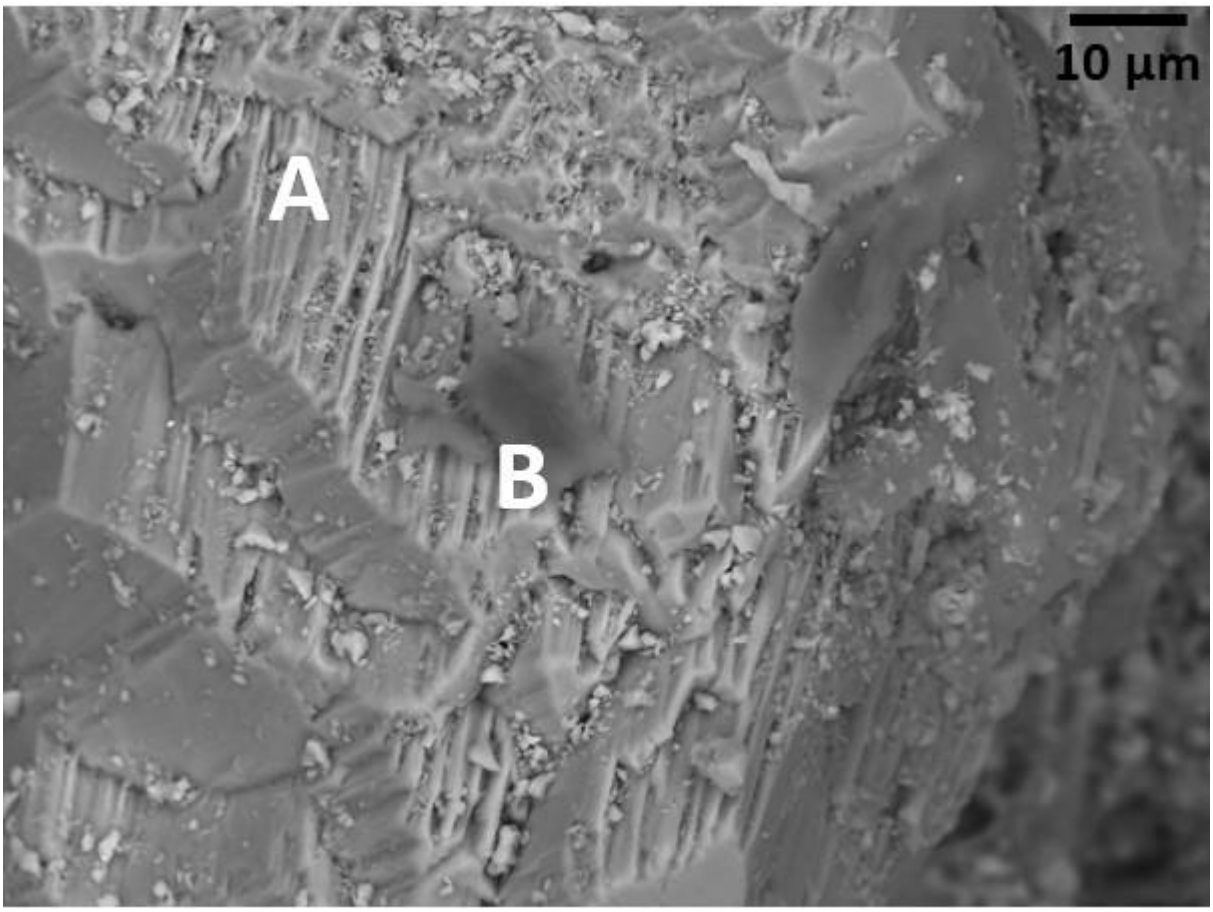

Figure 12: SEM image (BSE) of a cross section of the Saint-Denis SD limestone and associated Kα mapping of S.

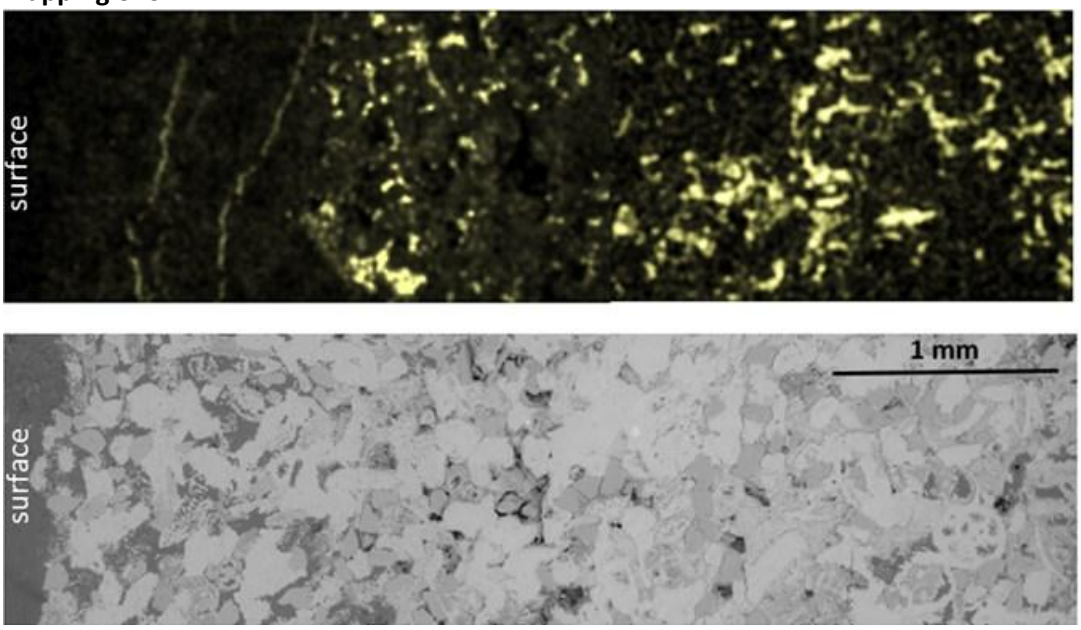

Figure 13: From the pristine to the weathered limestone: two possible evolutions of the surface and the subsurface.

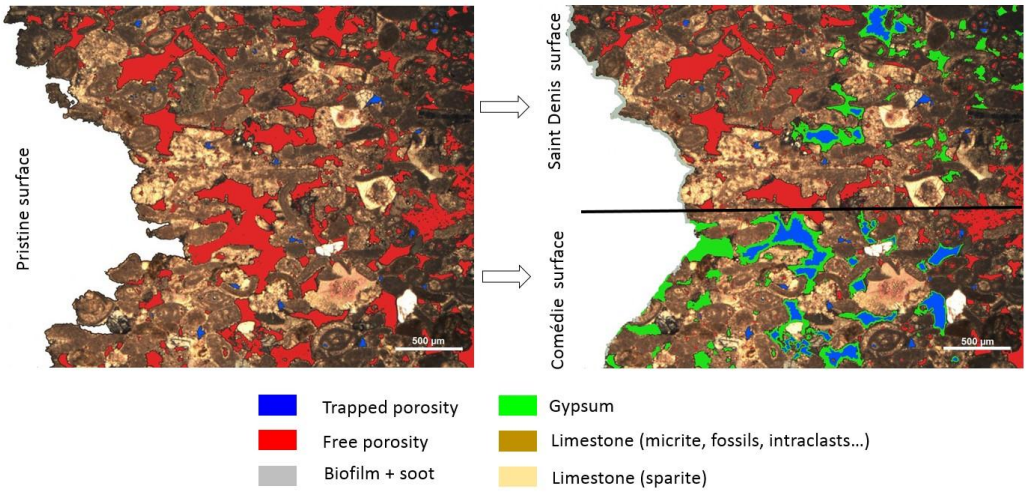

Table 1: Petrophysical parameters of the Saint-Maximin limestone (*: measurements on 3 samples). Pore throat radii 1 is the pore throat radii of the main mode corresponding to the macropores, and pore throat radii 2 is the pore throat radii of the secondary mode corresponding to the micropores.

Sample	Total porosity Nt* (%)	Water capillary coefficient A* ($g.cm^{-2}.h^{-0.5}$)	Porosity opened to mercury (%)	Pore throat radii 1 (µm)	Pore throat radii 2 (µm)
Q limestone	38.1±0.4	3.7±0.1	36.2	20	0.15
C limestone	41.7±2.1	1.9±0.7	40.4	10	3
SD limestone	30.7±1.0	0.5±0.1 to 2.4±0.4	27.6 to 33.9	10	3.5

Table 2: Semi-quantification of the phases identified at the surface of the samples using XRD.

Limestone type	Calcite (01-072-1937)	Quartz (04-075-0443)	Gypsum (00-033-0311)
Quarry Q	97%	3%	-
C	76%	12%	12%
SD	73%	18%	9%